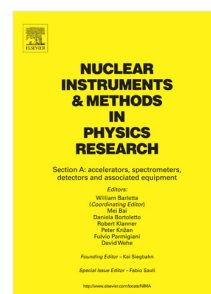# Accepted Manuscript

Fabrication and experimental evaluation of microstructured^{6}Li silicate fiber arrays for high spatial resolution neutron imaging

Michael E. Moore, Joris Lousteau, Pavel Trtik, Hassina Z. Bilheux, Diego Pugliese, Daniel Milanese, Angela T. Simone, Gilberto Brambilla, Jason P. Hayward

Please cite this article as:, Fabrication and experimental evaluation of microstructured^{6}Li silicate fiber arrays for high spatial resolution neutron imaging, *Nuclear Inst. and Methods in Physics Research, A* (2018), https://doi.org/10.1016/j.nima.2018.12.010

1 Fabrication and experimental evaluation of microstructured ^{6}Li silicate fiber arrays for high spatial

2 resolution neutron imaging

3

4 Michael E. Moore[a], Joris Lousteau[b], Pavel Trtik[c], Hassina Z. Bilheux[d], Diego Pugliese[e], Daniel Milanese[e],

5 Angela T. Simone[a], Gilberto Brambilla[b], Jason P. Hayward[a]

6

7 [a] Department of Nuclear Engineering, University of Tennessee, Knoxville, TN 37996, USA

8 [b] Optoelectronics Research Centre, University of Southampton, Southampton, SO17 1BJ, UK

9 [c] Laboratory for Neutron Scattering and Imaging, Paul Scherrer Institut (PSI), CH-5232 Villigen,

10 Switzerland

11 [d] Neutron Scattering Division, Oak Ridge National Laboratory, Oak Ridge, TN 37831, USA

12 [e] Department of Applied Science and Technology and RU INSTM, Politecnico di Torino, Corso Duca

13 degli Abruzzi 24, 10129 Torino, Italy

14

15 **Abstract**

16 This work presents the fabrication and experimental evaluation of instrumentation designed to enable

17 higher spatial resolution neutron radiography for those performing research at neutron scattering facilities.

18 Herein, we describe a proof-of-concept array of microstructured silicate fibers with ^{6}Li doped cores that

19 shows progress towards a design for μm resolution neutron radiography. The multicore fiber was fabricated

20 by drawing stacked unit elements of Guardian Glass (Nucsafe Inc., Oak Ridge, TN, USA), a ^{6}Li scintillating

21 core glass, and a silicate cladding glass. These structured fibers function as an array of sub-10-μm

22 waveguides for scintillation light. Measurements have shown a significantly increased integrated charge

23 distribution in response to neutrons, and the spatial resolution of the radiographs is described by edge

24 response and line spread functions of 48 ± 4 μm and 59 ± 8 μm, respectively.

25

28

1. Introduction

30

31   The properties of novel X-ray opaque materials, like those used in energy storage systems, precision

32 manufacturing technologies, aerospace components, and metallic additive manufacturing, are often

33 described using simulation tools lacking experimentally grounded models, and are based on first-principle

34 calculations and theoretical assumptions alone. Thus, ongoing material characterization relies on neutron

35 scattering instrumentation to verify performance predictions and add structure to future models. Despite the

36 successes that neutron scattering science facilities have achieved in recent years, even higher-impact

37 research into microstructure evolution, thermodynamic, and mechanical properties of advanced materials

38 is sometimes limited by the current spatial resolution of neutron sensing instrumentation.

39

40   Recent improvements in neutron sensing instrumentation have enabled a few modern neutron scattering

41 facilities to reach the current state-of-the-art spatial resolution of approximately 10-25 µm [1] [2]. However,

42 progress towards µm resolution remains a challenging goal for the neutron imaging community for two

43 primary reasons.

44

45   Firstly, thermal neutron fluxes at even the most novel user facilities are much lower than similar X-ray

46 imaging sources. For example, the raw power of several tens of W/cm^2 is regularly reported at advanced

47 X-ray sources like Advanced Photon Source (APS) at Argonne National Laboratory. This power

48 corresponds to a range of fluxes that conservatively start several orders of magnitude greater than the

49 estimated novel thermal neutron flux of approximately $1.2 \times 10^9 \ n/s/cm^2$ at the ODIN neutron imaging

50 beamline planned at the European Spallation Source (ESS) [3].

51

52   Secondly, the efficiency of thermal neutron sensitive scintillators is in competition with the spatial

53   resolution. Thick scintillators (mm scale) have higher efficiencies and, therefore, can produce high contrast

54   radiographs in less time than thin scintillators (µm scale). However, a thick scintillator will have poor spatial

55   resolution, as the position of captured neutrons is smeared throughout the scintillating volume. Conversely,

56   thin scintillating screens and films bypass spatial resolution smearing by reducing the thickness of

57   scintillating medium at the cost of efficiency. Still, the spatial resolution of unstructured thin scintillators is

58   fundamentally limited by the variance introduced by the difference in track orientations of the charged

59   particles emitted from neutron captures and the succeeding isotropic emission of scintillation light from

60   neutron converters such as ^{6}Li$(n, ^3H)$, ^{10}B(n, α), and ^{157}Gd(n, γ). Thus, there is a clear need to marry the

61   benefits of high efficiency and spatial resolution while also overcoming the neutron capture position

62   uncertainty that results from charged particle track variance. Some of our prior work based upon Monte

63   Carlo simulation suggests that tracking these charged particles on an event-by-event basis could allow one

64   to overcome this limiting uncertainty [2] [4].

65

66   Not long after the seminal work on neutron scintillating glasses [5] was published, scintillating fiber optic

67   glass faceplates were being researched for particle tracking applications in high energy physics experiments

68   in 1983 [6]. Three years later, the first results of a neutron scintillating fiber (SCIFI) tracker were reported

69   [7]. In 1994, the first neutron radiograph, of a pierced sheet of Gd, taken using a SCIFI array was published

70   with resolvable features on the order of several 100s of µm [8]. Since that time, SCIFIs have been

71   researched for remote radiation dosimetry and neutron sensitive fusion applications [9] [10] [11]. More

72   recently, interest surrounding coupling optical fiber tapers to existing scintillator based neutron imaging

73   setups has grown with novel 11 µm resolution results [1]. However, in the last 24 years, it appears that no

74   work has been done to build upon the original concept of the SCIFI tracker.

75

76   We propose the use of microstructured scintillating optical fiber arrays, capable of heavy charged particle

77 (HCP) tracking via waveguiding scintillation light following neutron capture, for high resolution neutron

78 imaging. Specifically, we utilize the well-known capture reaction for Li-glass ^{6}Li (n, α), emitting alpha (α)

79 and triton (^3H) particles back-to-back that ionize primary and secondary electrons, exciting a Ce^{3+}

80 activator, which in turn emits scintillation light at 395-432 nm in the near-UV/visible wavelength range.

81 This light is transported through the neutron sensitive microstructured waveguides and is observed by a

82 photodetector, see Figure 1. Provided that the collected and converted light has a sufficient signal to noise

83 ratio (SNR), one should be able to observe the tracks of these particles and precisely estimate the locations

84 of neutron capture reactions [4].

85

86   In our first generation proof-of-concept array, we attempted to use air capillaries in the cladding layer to

87 maximize the refractive index difference between the Li-doped glass core and the cladding. While the lead

88 oxide cladding glass was mechanically compatible with the Li core glass, the air capillaries tended to

89 collapse, so we moved to an all-solid glass design. With the all-solid design, we have made several attempts

90 to better match the thermal fiber pulling properties with the optical properties to achieve the best active

91 scintillating volume and refractive index difference insofar as possible. This work describes the fabrication

92 and characterization of this next generation, proof-of-concept neutron SCIFI tracker.
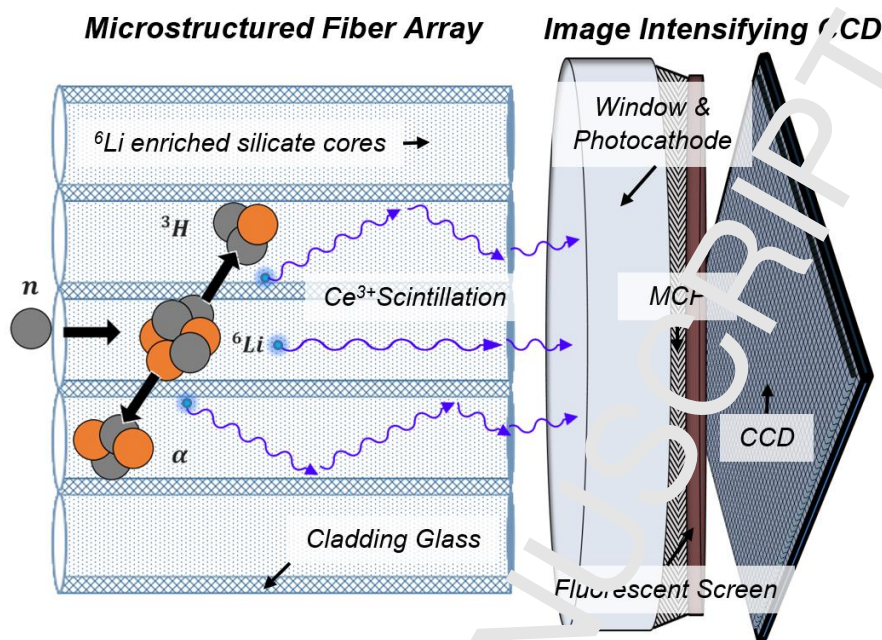
93

94

95 Figure 1. Enriched lithium-6 glass fibers that are doped with cerium absorb thermal neutrons, emit scintillation light,

96 and act as optical waveguides to channel the scintillation light for imaging. They are surrounded by a cladding of

97 lower refractive index. While an image intensifying CCD is our selected choice for a photosensor in this proof-of-

98 concept study, it is possible that a different photosensor may be more appropriate in order to scale to a larger area.

99

100 ## 2. Fabrication

101

102   To fabricate the neutron SCIFI, a multicore design was used. A rod of ^{6}Li-loaded glass with properties

103 similar to GS20 [5] (fabricated by Nucsafe Inc., Oak Ridge, TN, USA) was inserted in an extruded optical

104 glass cladding tube. Canes of Li-glass cores, embedded in the optical cladding glass, were drawn and then

105 stacked into an array of some geometry. This array of canes, the preform, was pulled into a single multicore

106 fiber. For this neutron SCIFI to act as a successful waveguide, the refractive index of the core, n_{co}, must

107 be larger than the cladding refractive index, n_{cl}. While Li-glass has $n_{co} = 1.55$, a desirable cladding

108 candidate should have $n_{cl} \leq 1.5$ [7]. Additionally, to create a uniform and regular microstructure, the glass

109 viscosities must be matched for fiber drawing. Previous trials of ours have led to a better understanding of

110 difficulties associated with matching both optical and thermal properties of glass fiber while maintaining

111 the chemical stability required for scintillation. An early attempt to create a square multicore neutron SCIFI,

112 described in detail in [12], yielded an irregular array of cores that had a refractive index almost equal to the

113 chosen cladding. Although drawing was possible, issues related to glass devitrification during fiber pulling

114 significantly decreased the fiber guiding properties, undermining the neutron resolution. Alternatively, the

115 N-FK5 SCHOTT glass makes a more attractive cladding glass with an n_d equal to 1.5 and a seemingly

116 compatible transition temperature, (T_g). However, our initial canes of Li-glass and N-FK5 crystallized

117 during drawing due to an incompatible codrawing temperature for the glass viscosities.

118

119   The fabrication of our current multicore fiber began with the extrusion of an N-KF9 cladding tube. A

120 cylindrical glass billet with a 29 mm diameter and 35 mm height and a stainless steel die was used during

121 the extrusion process. A 4 kN force was applied to the die and the glass billet while the glass was held in a

122 furnace at an onset temperature of 650°C (true glass temperature of 620°C). Some metallic inclusions were

123 observed inside the extruded glass. Next, the Li-glass rod (11.7 mm diameter) was inserted into a 100 mm

124 long section of the extruded N-KF9 tube, and drawn using the preform drawing method. To determine the

125 optimal drawing temperature, the Li-doped silicate glass, T_g, was experimentally established with

126 differential scanning calorimetry (Netzsch DSC STA 449 F1 JUPITER). The measurement was carried out

127 with a heating rate of 5°C/min up to 1300°C in sealed Pt/Rh pans using ~ 30 mg of fine grain sample,

128 providing a value of T_g = 470 ± 2°C. So, the fiber drawing took place at a furnace onset temperature of 800

129 °C (730 ±10°C glass temperature) under a flow of N_2 at 2 l/min. The preform was fed into the furnace at

130 a speed of 1 mm/min, and the fiber was drawn at a speed of 5.4 m/min under a tension of 15 g. About 500

131 m of fiber were drawn from the preform, resulting in a fiber with an outer diameter and a core diameter of

132 185 ±4 μm and 50 ±4 μm, respectively.

133

134   The fiber was then cut into 2,700 separate 120-mm-long pieces and stacked as a hexagonal array. This

135   array was then thermally consolidated into a single unit at 640°C and the N-KF9 tube (12 ±0.2 mm OD/

136   11.4 ±0.2 mm ID), used to jacket the Li-glass cores, was extruded under the same conditions previously

137   described for the outer cladding tube. The resulting preform was then drawn into a single multicore fiber

138   910 ±10 µm in diameter with individual cores possessing 7–10 µm diameters, see Figure 2. The hexagonal

139   circle packing geometry allows for the highest fill fraction (active scintillating volume) of circles (cores) to

140   remaining space (cladding), $\frac{\pi\sqrt{3}}{6} \approx 90.7\%$, provided the pitch of cores is equal to the diameter of the cores.

141   Given a conservative estimate of the average cladding spacing between cores of ~2 µm, we estimate that

142   the active scintillating volume of our hexagonal multicore structure is ≈ 70%. Thus, we have found that

143   this multicore design enables uniform core spacing at a 70% active volume, while also allowing for sub-

144   10-µm individual core dimensions.

145

146

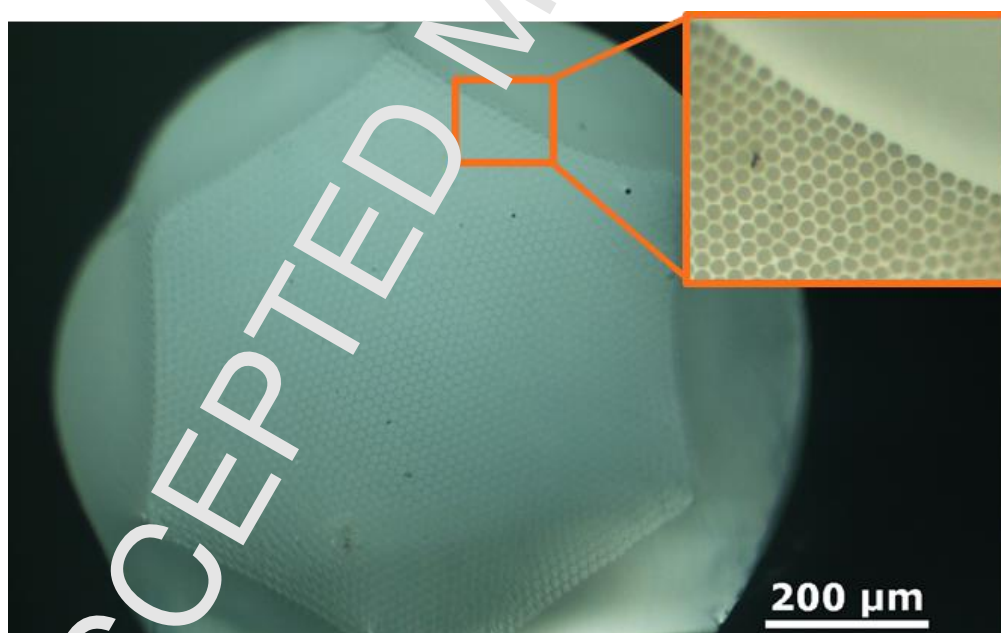147   Figure 2. Photographed cross section of a cleaved end of a single multicore SCIFI (hexagonal) inside of its outer

148   jacket (round)

3. Experimental Evaluation

Following fiber drawing, it is necessary to establish that our neutron SCIFI still scintillates as expected. Thus, the radioluminescence emission spectrum of an unpolished Li-glass rod, used for the core glass, was measured for an *On Side* (diameter) and an *On End* (length) case. The diameter of the unpolished Li glass rod was 10 mm with a length of 150 mm. A standard emission peak of Ce^{3+} scintillation light near to the 395 nm peak emission was observed for the *On Side* case, see Figure 3. For the *On End* case, the emission peak contracted 15 nm in the near-UV region. Here, the self-absorption effects of the overlapping Ce^{3+} and Ce^{4+} emission and absorption bands are observed when the scintillation light is transported further for the *On End* case. In Figure 3, these unpolished rod results are compared to the arrays of multicore SCIFIs, with and without the outer jacket removed; refer back to Figure 2 for an image of a single multicore fiber possessing an outer jacket. The SCIFI arrays were 2 mm thick with a 5 x 5 mm surface. The SCIFI arrays were measured on end, as a faceplate. After undergoing the aforementioned heat processing, the SCIFI

162 emission behaves as expected for Ce^{3+} scintillation. The SCIFI had a slightly broadened emission, 3-5 nm,
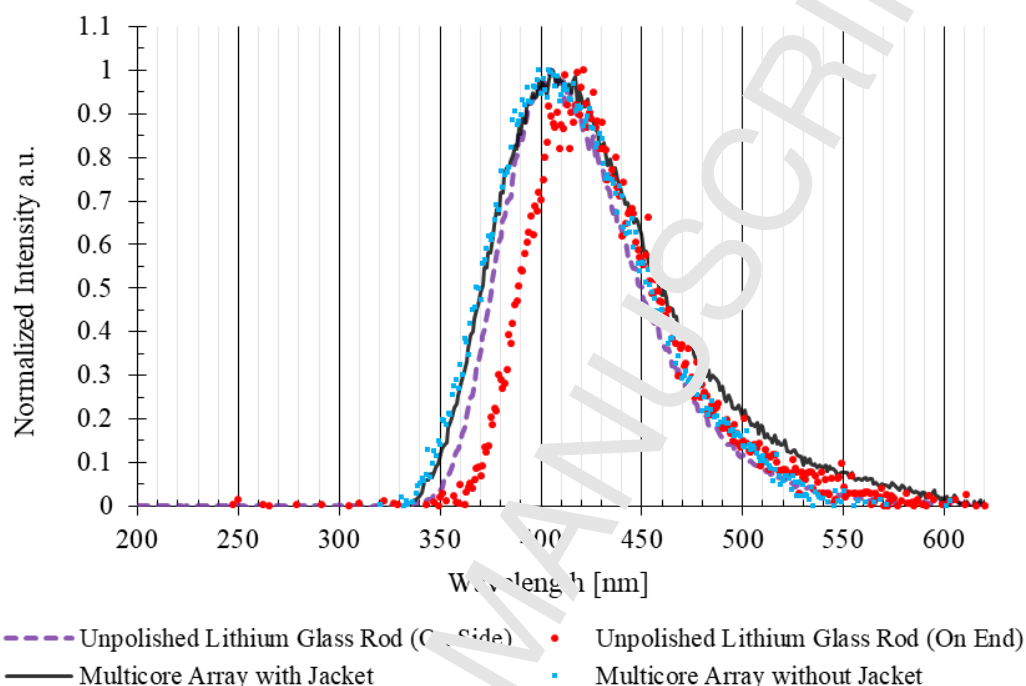
163 compared to the *On Side* case for the Li-glass rod.

164

Unpolished Lithium Glass Rod (On Side)   Unpolished Lithium Glass Rod (On End)
Multicore Array with Jacket   Multicore Array without Jacket

165

166 Figure 3. Radioluminescence spectra characteristic of Ce^{3+} activator emission for the unpolished ^{6}Li glass rod

167 (unprocessed) and the multicore arrays (drawn into fibers) with and without outer jackets.

168

169   Having verified that the scintillation mechanism is behaving as expected, it is essential to characterize

170 any transport of the Ce activator from the core to the cladding via thermal diffusion to ensure that

171 scintillation light is being produced within the core glass. So, Energy Dispersive X-ray Spectrometry (EDS)

172 was used to examine the atomic concentrations of dopants in cane cross-sections with a Zeiss EVO MA15

173 Scanning Electron Microscope. The canes of the Li-glass cores cladded with N-KF9 were embedded in

174 epoxy, and EDS line scans were acquired across the ends of the canes. The results of the EDS line scans

175 are shown in Figure 4, where Mg inside of the core glass can be seen as the boundary between the core and

176 cladding. No decrease, below standard deviation, for the Ce concentration in Li-glass cores at the near-

177 cladding position was observed. EDS point scans targeting 4 randomly selected Li-glass cores, at 3 positions

178 each, correctly detected a Ce concentration of 2.4 $\pm$0.2 wt.%. No Ce was detected when point scans targeted

179 the cladding with a lower detectable limit set to 0.1 wt.%. So, the intensity of the Ce concentration in the

180 cladding and surrounding epoxy is assumed to be background. Thus, Ce was well bound within the core

181 glass during fiber drawing. Again, the fiber was drawn at a 730 $\pm$10°C glass temperature, 260°C above T_g,

182 with any given segment of fiber experiencing approximately 10 min of heating. Previous work of ours has

183 shown that the mobility of Ce in Li-glass, heated at temperatures between 500-600°C for 5 hr with a

184 subsequent 24 hr anneal, resulted in a few μm of Ce diffusion [13]. Thus, the quasi-immobilization of Ce

185 for the short heating duration agrees with our experimental data.

186

187   If a significant quantity of the ^{6}Li absorber is in the SCIFI cladding, then neutron captures in the cladding

188 could decrease overall light output, and potentially create $\pm$ 5 μm position smearing. So, it useful to know

189 how the ^{6}Li absorber is diffusing within the multicore. However, EDS systems are fundamentally

190 insensitive to atomic numbers < 5 due to the absorption of low energy X-rays within the detection window.

191 X-Ray Photoelectron Spectroscopy could be used to search for Li in the cladding, but it would not provide

192 an accurate concentration depth profile. Such a technique would require micron scale accuracy when

193 removing core from cladding, and while probing the depth of the cladding. Instead, the mobility of another

194 alkali metal, Na, is particularly interesting because of its chemical similarity, comparable ionic radius, and

195 mobility to the Li absorber in the core glass. The diffusion of Na within Li enriched silicate, ^{7}Li/^{6}Li =

196 0.04526, and Na self-diffusion within 0.33 Na$_2$O, 0.67 SiO$_2$ glass has been shown to be closely comparable

197 [14] [15]. Additionally more recent analysis indicates that the activation energy for Li diffusion remains

198 comparable to Na, specifically inside of aluminosilicate glasses; where mixed alkali effects will not

199 immobilize Li or Na [16] [17]. The self-diffusion of Na within the cladding glass and its diffusion of 30 $\pm$4

200 μm into the core can be clearly seen in Figure 4. Although the EDS line scan intensities do not represent

201 relative concentrations between elements, the Li absorber is very likely diffusing in a similar manner to Na

202 from the core into the cladding.
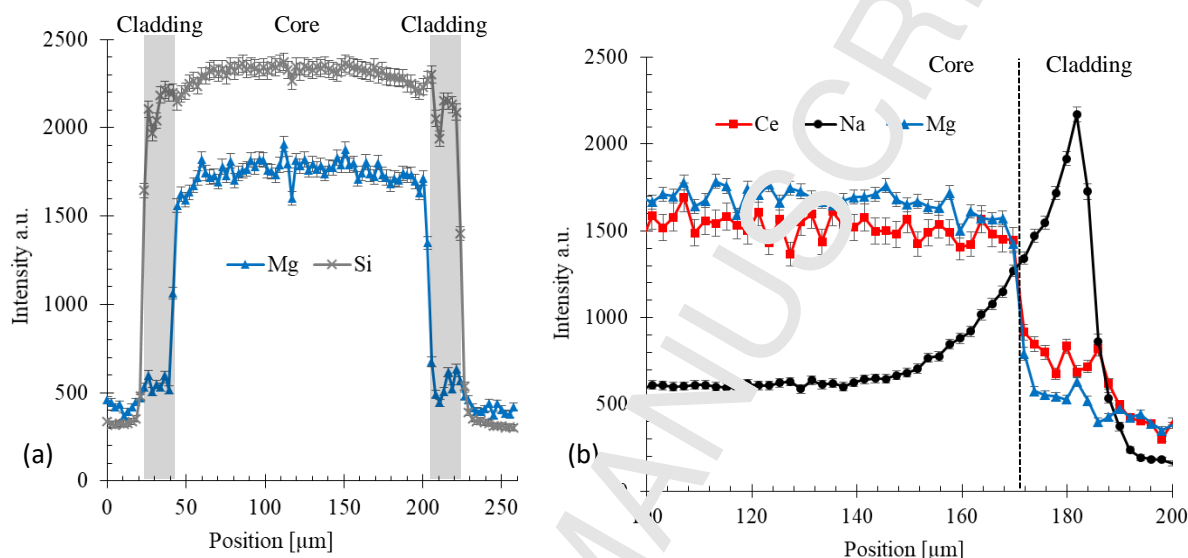
203

204

205

206 Figure 4. (a) EDS line scan across the entire cane where the core (Mg) and core/cladding (Si) components can be

207 seen, and (b) spectra of the core-cladding interface for Mg, Ce, and Na.

208

209 Preliminary studies on gamma/neutron discrimination performance of the Li-glass within the previous

210 square multicore SCIFI described in [12], were conducted at the CG-1D neutron imaging beamline at the

211 High Flux Isotope Reactor (HFIR) at Oak Ridge National Laboratory (ORNL) [18]. The response of the

212 previous square multicore SCIFI array to background radiation (cold neutron flux $< 1 \times 10^1 \ n/s/cm^2$ at

213 target with neutron shutter closed), and to the neutron beam (cold neutron flux at $\sim 1 \times 10^7 \ n/s/cm^2$ at

214 target with neutron shutter open) was observed with an R9779 PMT. The scintillation light was separable

215 from electronic noise or Cherenkov light generated in the PMT window, both in magnitude (integrated

216 charge) and fall time where the longer fall times are characteristic of scintillation caused by the Ce^{3+} dopant.

217 While scintillation was clearly seen for both cases, the response to the neutron beam displayed an increased

218 integrated charge distribution as the array exhibited a higher light output response to cold neutrons than the

219   gamma background radiation present in the beamline. Due to the low effective active scintillating volume

220   of the previous square packing used (~27%), the majority of energy deposited in the multicore from the

221   charged particles was not producing scintillation light. The current hexagonal design allows for nearly triple

222   the amount of energy to be deposited into the scintillating core glass.

223

224   Radiographs were taken with the current hexagonal multicore fibers using the Swiss Spallation Neutron

225   Source at the Paul Scherrer Institut (PSI). Images were acquired with the Neutron Microscope (NM) at the

226   Pulse OverLap DIffractometer (POLDI) beamline. The use of the NM at the POLDI beamline was uniquely

227   desired due to the requirements of the optical system needed for this experiment. Specifically, the NM

228   possesses the magnification and numeric aperture to enable a nominal pixel size of acquired images of 1.3

229   μm, and a true spatial resolution of about 5 μm [19]. Additionally, the optics have μm-level repeatable

230   positioning, and are sensitive to near UV Ce scintillation. Using the NM at the POLDI beamline is also

231   beneficial due to a lower gamma background compared with other beamlines, a thermal/cold neutron

232   spectrum from 1.1–5 Å, and a flux at the sample position of $6 \times 10^6 \; n/s/cm^2$ [20].

233

234   A diffused, blue light source was used to optically focus onto the ends of hand-cleaved and polished

235   single multicore fibers. Al tape was then used to enclose the scintillator. Open Beam (OB) images were

236   taken to focus the optics to the scintillation light. A quantity of 20 images with 300 s exposures were

237   acquired of the OB. A gadolinium-based Siemens Star (SS) [21] was then positioned in front of the active

238   area of the scintillator and imaged. Eighty (80) images of the SS with 300 s exposure were acquired. Due

239   to decreased thermal neutron flux, 2 OB and 11 SS images were removed prior to post processing. The

240   remaining SS images, with outliers removed, were divided by the OB background, and summed. The

241   resultant image was transformed with a bilinear clockwise rotation of 90° for analysis. The resolvable

242   spokes of the SS can be seen in Figure 5. The resolution of the 2 mm fiber can be estimated via inspection

243   of the highlighted region of the SS spokes possessing approximately 50 μm spatial features. Referencing

244   the 10% to 90% contrast transition for the Edge Response Function (ERF) of the spoke in the highlighted

245 region, a 48 ±4 µm resolution was found. Fitting a Gaussian to the Line Spread Function (LSF) of the same

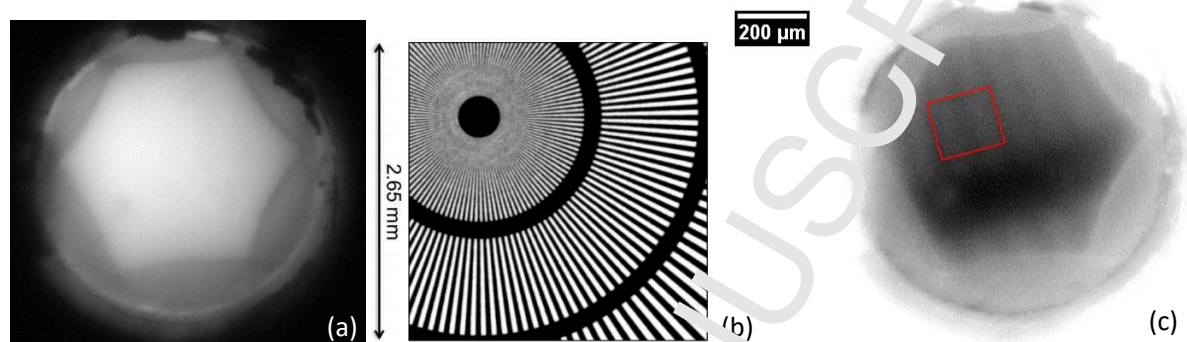246 region, a FWHM measurement yields 59 ±8 µm spatial resolution.

247

248

Figure 5. (a) OB neutron radiograph taken with a 2 mm thick multicore neutron SCIFI, (b) visual test object reference, PSI's Gd SS taken with the NM in [18], and (c) neutron radiograph of the SS acquired after aforementioned post processing, with the region of interest highlighted.

4. Conclusions and Future Work

Li-glass cores with 7-10 µm diameter have been drawn into 500 m of an all-solid glass composite, multicore fiber at a 70% packing fraction. The Li-glass remains active and scintillates as expected following drawing. The Li absorber shows some diffusion into the cladding, but the Ce activator is largely bound during the fabrication process. Hand-cleaved and polished single fibers of lengths 2-5 mm have resolved features on the order of 10's of µm while utilizing the Neutron Microscope. Ideal light collection in these same fibers should allow for ≤ 20 µm resolution. To increase spatial resolution, the core glass must be drawn to smaller sizes which should be possible with the current fabrication process. Image contrast

263 improvement requires the use of a lower refractive index cladding material. Moreover, fabrication without

264 an outer cladding jacket will allow for easy array assembly.

265

266   Near term work is planned to evaluate the radiographic spatial resolution of an array of 100 multicore

267 neutron SCIFIs with a 5 x 5mm field-of-view. This is a comparably thinner design (1mm thick), with outer

268 jacket removed, and it has a well-polished surface. Since a larger field-of-view was desired for evaluation

269 of imaging performance, the multicore fiber outer jacket was ground away, and a 10×10 array was stacked

270 together. Assembly was finished by securing the array with structural glass plate siding and polishing the

271 surfaces, see Figure 6.

272

273   Meanwhile, a novel phosphate glass cladding, possessing a refractive index of $n_c < 1.53$, is being used

274 for another neutron SCIFI fabrication. This cladding is expected to allow for more than twice the current

275 amount of scintillation light to remain internally bound. We plan to draw the multicore fiber using the

276 phosphate cladding with a goal of 2 μm diameter Li glass cores while remaining at a packing fraction ≥
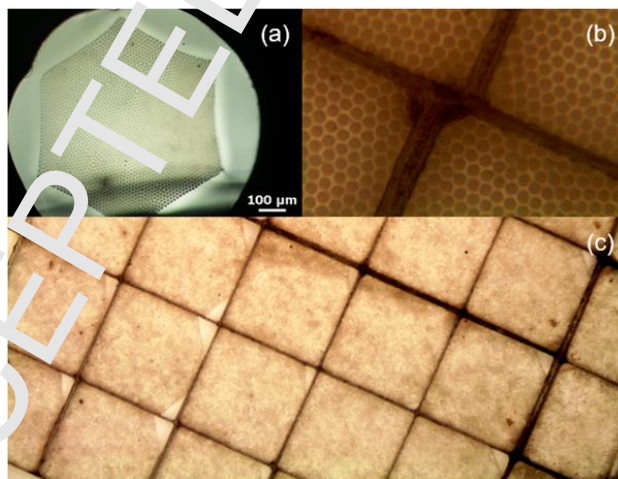
277 70%.

278

279 Figure 6. Microscope photos of the (a) cross section of a microstructured multicore fiber with scale, (b) stacked

280 multicore fiber with outer cladding removed with 8 ± 1 μm core diameters, and (c) polished faceplate surface of a

281 multicore SCIFI array with 0.5 x 0.5 mm pixels

References

[1]   M. Morgano, et al. "Unlocking high spatial resolution in neutron imaging through an add-on fibre optics taper." *Optics Express* 26.2 (2018): 1809-1816.

305 [2] A.S. Tremsin, et al. "Neutron radiography with sub-15 μm resolution through event centroiding."

306 *Nuclear Instruments and Methods in Physics Research Section A: Accelerators, Spectrometers,*

307 *Detectors and Associated Equipment* 688 (2012): 32-40.

308 [3] M. Strobl. "The scope of the imaging instrument project ODIN at ESS." *Physics Procedia* 69

309 (2015): 18-26.

310 [4] Y. Song, et al. "Monte Carlo simulation of a very high resolution thermal neutron detector

311 composed of glass scintillator microfibers." *Applied Radiation and Isotopes* 108 (2016): 100-107.

312 [5] A. R. Spowart. "Neutron scintillating glasses: Part 1. Activation by external charged particles and

313 thermal neutrons." *Nuclear Instruments and Methods* 135 (1976): 441-453.

314 [6] R. Ruchti, et al. "A Scintillating Glass, Fiber-Optic Plate Imaging System for Active Target and

315 Tracking Applications in High Energy Physics Experiments." *IEEE Transactions on Nuclear*

316 *Science* 30.1 (1983): 40-43.

317 [7] M. Atkinson, et al. "Initial tests of a high resolution scintillating fibre (SCIFI) tracker." *Nuclear*

318 *Instruments and Methods in Physics Research Section A: Accelerators, Spectrometers, Detectors*

319 *and Associated Equipment* 254.2 (1987): 500-514.

320 [8] P. Ottonello, et al. "Slow neutron imaging using scintillating glass optical fibers." *Nuclear*

321 *Instruments and Methods in Physics Research Section A: Accelerators, Spectrometers, Detectors*

322 *and Associated Equipment* 349.2-3 (1994): 526-531.

323 [9] N. Miyanaga, N. Ohba, and K. Fujimoto. "Fiber scintillator/streak camera detector for burn history

324 measurement in inertial confinement fusion experiment." *Review of scientific instruments* 68.1

325 (1997): 621-623.

326 [10] A. Vedda, et al. "Ce3+-doped fibers for remote radiation dosimetry." *Applied physics letters* 85.26

327 (2004): 6356-6358.

328 [11] N. Chiodini, et al. "Ce-doped SiO_2 optical fibers for remote radiation sensing and measurement."

329 *Fiber Optic Sensors and Applications VI*. Vol. 7316. International Society for Optics and Photonics,

330 2009.

331 [12] M.E. Moore, et al. "A multicore compound glass optical fiber for neutron imaging." *Optical Fiber*

332   *Sensors Conference (OFS), 2017 25th*. IEEE, 2017.

333 [13] M.E. Moore, et al. "Thermal diffusion of mixed valence Ce in ^{6}Li loaded silicate glass for neutron

334   imaging." *Journal of Non-Crystalline Solids* 498 (2018): 145-152.

335 [14] G.H. Frischat. "Sodium diffusion in SiO2 glass." *Journal of the American Ceramic Society* 51.9

336   (1968): 528-530.

337 [15] W. Beier and G. H. Frischat. "A mass spectrometric method for the determination of Li self

338   diffusion in oxide glasses." *Journal of Non-Crystalline Solids* 38 (1980): 569-573.

339 [16] W. Li, and S.H. Garofalini. "Molecular dynamics simulation of lithium diffusion in Li2O–Al2O3–

340   SiO2 glasses." *Solid State Ionics* 166.3-4 (2004): 365-273.

341 [17] J.O. Isard. "The mixed alkali effect in glass." *Journal of Non-Crystalline Solids* 1.3 (1969): 235-

342   261.

343 [18] L. Santodonato, et al. "The CG-1D neutron imaging beamline at the oak Ridge National

344   Laboratory high flux isotope reactor." *Physics Procedia* 69 (2015): 104-108.

345 [19] P. Trtik, and E. H. Lehmann. "*Progress in High-resolution Neutron Imaging at the Paul Scherrer*

346   *Institut-The Neutron Microscope Project.*" *Journal of Physics: Conference Series,* vol. 746. No. 1.

347   IOP Publishing, 2016.

348 [20] U. Stuhr, et al. "Time-of-flight diffraction with multiple frame overlap Part II: The strain scanner

349   POLDI at PSI." *Nuclear Instruments and Methods in Physics Research Section A: Accelerators,*

350   *Spectrometers, Detectors and Associated Equipment* 545.1-2 (2005): 330-338.

351 [21] C. Grünzweig, et al. "Highly absorbing gadolinium test device to characterize the performance of

352   neutron imaging detector systems." *Review of Scientific Instruments* 78.5 (2007): 053708.

353